



This is a repository copy of *Electrically injected hybrid organic/inorganic III-nitride white light-emitting diodes with nonradiative Förster resonance energy transfer*.

White Rose Research Online URL for this paper:  
<http://eprints.whiterose.ac.uk/133649/>

Version: Published Version

---

**Article:**

Ghataora, S., Smith, R.M. [orcid.org/0000-0002-7718-7796](https://orcid.org/0000-0002-7718-7796), Athanasiou, M. et al. (1 more author) (2018) Electrically injected hybrid organic/inorganic III-nitride white light-emitting diodes with nonradiative Förster resonance energy transfer. *ACS Photonics*, 5 (2). pp. 642-647. ISSN 2330-4022

<https://doi.org/10.1021/acsp Photonics.7b01291>

---

© 2018 American Chemical Society. ACS AuthorChoice - This is an open access article published under an ACS AuthorChoice ([http://pubs.acs.org/page/policy/authorchoice\\_termsfuse.html](http://pubs.acs.org/page/policy/authorchoice_termsfuse.html)) which permits copying and redistribution of the article or any adaptations for non-commercial purposes.

**Reuse**

Items deposited in White Rose Research Online are protected by copyright, with all rights reserved unless indicated otherwise. They may be downloaded and/or printed for private study, or other acts as permitted by national copyright laws. The publisher or other rights holders may allow further reproduction and re-use of the full text version. This is indicated by the licence information on the White Rose Research Online record for the item.

**Takedown**

If you consider content in White Rose Research Online to be in breach of UK law, please notify us by emailing [eprints@whiterose.ac.uk](mailto:eprints@whiterose.ac.uk) including the URL of the record and the reason for the withdrawal request.



[eprints@whiterose.ac.uk](mailto:eprints@whiterose.ac.uk)  
<https://eprints.whiterose.ac.uk/>

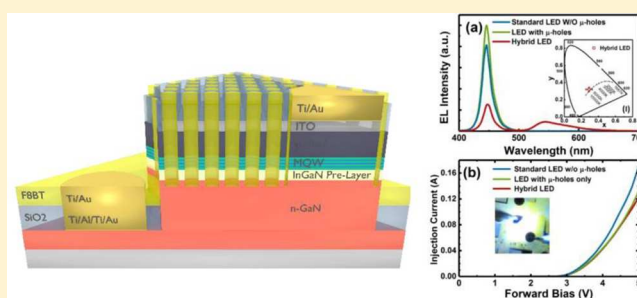
# Electrically Injected Hybrid Organic/Inorganic III-Nitride White Light-Emitting Diodes with Nonradiative Förster Resonance Energy Transfer

Suneal Ghataora, Richard M. Smith, Modestos Athanasiou, and Tao Wang\*

Department of Electronic and Electrical Engineering, The University of Sheffield, Mappin Street, Sheffield, S1 3JD, United Kingdom

**ABSTRACT:** An electrically injected hybrid organic/inorganic III-nitride white light-emitting diode (LED) has been fabricated by using a two-dimensional (2D) microhole array structure. The hybrid LED geometry significantly enhances proximity between the inorganic active-region and the down-converting yellow organic light-emitting polymers (OLEPs), enabling the near-field nonradiative Förster resonance energy transfer (FRET) process with high efficiency while retaining excellent electrical characteristics of an unpatterned planar LED. A reduction in the recombination lifetime in the InGaN/GaN blue active region has been observed with the hybrid device, confirming the nonradiative FRET process occurring between the InGaN/GaN blue active region and the yellow organic polymer. This results in a typical FRET efficiency of 16.7%, where the FRET interaction area accounts for approximately 0.64% of the remaining blue-emitting inorganic LED, but enhancing total device efficiency. An optimized white-light EL emission is achieved with typical CIE color coordinates at (0.29, 0.32).

**KEYWORDS:** InGaN/GaN emitters, organic emitters, nonradiative recombination lifetime, hybrid white LEDs, microhole arrays



Analogous to the technological development of the conventional telephone to smartphones, lighting is expected to experience a similar evolution leading toward “smart-lighting” that is utilized simultaneously in general illumination and ultrafast high-bandwidth visible light communication (VLC, i.e. Li-Fi). In this case, a white light source of special characteristics is required in order to meet the multiple-function requirements.

The last two decades have seen tremendous progress in developing solid-state lighting, based primarily on III-nitride semiconductors. So far, the current state-of-the-art remains founded on the well-known “blue LED + yellow phosphor” approach, depending on blue emission from InGaN/GaN LEDs radiatively pumping down-conversion phosphor materials that provide longer-wavelength yellow emission that generate together white lighting. However, the approach has a number of drawbacks, such as the self-absorption of the phosphor, limiting the color-conversion efficiency from blue to yellow wavelengths and thus severe color rendering issues, the issues on quenching and stability of the phosphors, and so on. Furthermore, another fundamental limitation for the utilization of such a white LED is due to the very slow response time of phosphors, typically on the order of microseconds, restricting the bandwidth to below 1 MHz for Li-Fi applications.<sup>1</sup> A receiver however would typically use blue filters to remove the slow-response of the phosphors’ yellow light,<sup>2</sup> resulting in a significant loss (~50%) to signal intensity.

Organic light-emitting polymers (OLEPs) have been developed rapidly in recent years due to a number of

advantages, such as high luminescence efficiencies, solubility, low cost manufacturing and flexibility. Furthermore, the much faster response times of organic materials, in comparison to existing phosphors, offers particular advantages in ultrafast Li-Fi.<sup>3</sup> OLEPs however suffer from a number of fundamental problems, in particular poor electrical properties. A hybrid organic/inorganic III-nitride white LED therefore combines the complementary advantages of the two major semiconductor material groups. The basic arrangement achieving white light emission involves the partial down-conversion of an electrically injected blue InGaN/GaN LED by yellow OLEP. A resulting hybrid device therefore features the respective high-performance electrical properties, ultrafast response and photoluminescent (PL) quantum yield of the inorganic and organic material systems,<sup>4</sup> expecting to demonstrate superior performance to current state-of-the-art white LEDs.

The issues of self-absorption are also eliminated by using OLEPs as a result of their intrinsically large Stokes-shift (>100 nm).<sup>5</sup> Unlike any existing phosphors which are normally prepared in a form of grains with a typical size of tens of micrometer, OLEPs can be dissolved in a solvent, obtaining homogeneous microstructures simply by means of standard spin-coating techniques widely used in the field of semiconductor optoelectronics. OLEPs can therefore simplify the process of fabricating white LEDs, which is particularly attractive to industry.

**Received:** October 30, 2017

**Published:** November 20, 2017

The most significant benefit using OLEPs instead of phosphors as down-conversion materials is that the efficiency of the color conversion can be significantly enhanced through a nonradiative Förster resonant energy transfer (FRET) mechanism,<sup>5–16</sup> which cannot be achieved using any existing phosphors. The organic down-conversion material then emits radiatively at a rate above nonradiative FRET rate, effectively stopping a reverse transfer process.<sup>12</sup> This avoids intermediate steps preceding the PL of the down-conversion material, which before absorption includes the photon emission and then extraction in a LED. The energy transfer process consequently generates a change in carrier recombination dynamics, resulting in an enhancement in total device efficiency, where the nonradiative FRET rate is sufficiently fast to suppress the nonradiative recombination processes in the inorganic LED.<sup>5</sup>

Nonradiative FRET involves a near-field radiation-less energy transfer from inorganic active-regions (donors) to OLEPs (acceptors) through dipole–dipole Coulombic interactions.<sup>14</sup> Therefore, it is crucial to ensure that the separation of donor and acceptor excitons is sufficiently small (typically <10 nm) in order to achieve a maximal conversion efficiency.<sup>5–10</sup> Previous attempts to employ nonradiative FRET are exclusively based on a single quantum well structure with a very thin capping layer of only several nanometers.<sup>6–14</sup> However, this form of structure cannot be fabricated into an electrically injected white LED due to the requirement of a thin (<15 nm) p-GaN layer, while a standard InGaN/GaN multiple quantum wells (MQWs) based blue LED typically has a ~200 nm p-GaN cap GaN. An electrically injected hybrid organic/inorganic white LED of this form has been demonstrated previously,<sup>7</sup> where the deposition of an OLEP above the standard blue LED replaces a yellow phosphor without introducing any nonradiative FRET process at all.<sup>18,19</sup>

In this paper, we report the fabrication of a 2D microhole array structure through the InGaN/GaN MQW of a standard blue LED, producing for the first time an electrically injected hybrid organic/inorganic white LED compatible with the near-field requirements of FRET. The LED geometry improves proximity between the inorganic active-region and a down-conversion OLEP, enabling a highly efficient near-field nonradiative FRET process while retaining excellent electrical characteristics. A reduction in the carrier recombination lifetime in the InGaN/GaN MQWs has been observed with organic/inorganic hybridization, demonstrating a FRET efficiency of 16.7%, where the FRET interaction area accounts for approximately only 0.64% of the remaining blue emitting inorganic LED, enhancing total device efficiency.

The geometric configuration designed for the new type of hybrid white LEDs aims to minimize the separation between donor and acceptor dipoles using a top-down fabrication of a 2D microhole array structure within a standard planar LED device. A down-conversion yellow OLEP is used to fill the volume of the 2D microholes, allowing adjacent coupling with the exposed InGaN/GaN MQW side-walls. As a consequence, an inherently continuous p-GaN layer is also maintained, ensuring the electrical properties of the unpatterned device.

Planar-LEDs with a standard size of  $350 \times 350 \mu\text{m}^2$  are initially fabricated here from a commercial blue InGaN/GaN LED wafer grown on c-plane sapphire, which consists of a  $1 \mu\text{m}$  n-GaN layer with a thick undoped GaN buffer on a standard thin low-temperature GaN nucleation layer, a 100 nm InGaN prelayer, then an 160 nm InGaN/GaN MQW active region and a final 230 nm p-GaN layer. A fabrication process for standard

planar LEDs is used. As usual, an initial mesa-etching is performed, meaning that part of the wafer is etched down to the n-GaN layer for the fabrication of n-contact later on. A 100 nm ITO (indium–tin-oxide) layer is then deposited across the remaining p-type region, forming an Ohmic contact after thermally annealing at 600 °C for 60 s in air. The n-contact electrode consists of Ti/Al/Ti/Au (20/100/20/60 nm). Finally, Ti/Au (20/200 nm) bond-pads are deposited on both the p-type and n-type contacts.

A 2D microhole array structure is then fabricated through the active-region using a combination of standard photolithography techniques and then a selective dry-etching process. The exposed active-region along the microhole circumference ensures a minimized separation between donor and acceptor dipole, where the nonradiative FRET interaction volume becomes the outer radius of the remaining InGaN/GaN MQW structure.<sup>5</sup> This significantly enhances the coupling between adjacent donor dipoles (i.e., InGaN/GaN MQWs) and acceptor dipoles (i.e., OLEP). The micrometer-scale used also matches the requirements of any standard lithography technique in terms of resolution.<sup>9</sup>

Figure 1a depicts a schematic of our hybrid LED with a 2D microhole array structure. The top-down process used for the

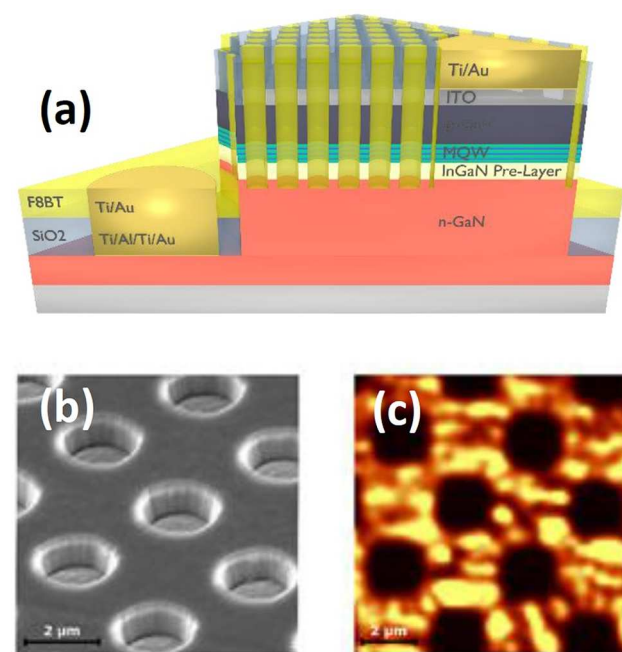


**Figure 1.** (a) Schematic diagram of the hybrid organic/inorganic white LED with a 2D microhole array structure; (b) SEM image of the 2D microhole array structured blue LED after etching through the InGaN/GaN MQWs (at 45° angle); and (c) High spatial-resolution confocal PL mapping of the InGaN/GaN MQWs, which is consistent with the microhole array patterning.

fabrication of 2D microhole arrays begins with a 250 nm SiO<sub>2</sub> layer deposited across the fabricated planar-LED using plasma-enhanced chemical vapor deposition (PECVD), before 20 nm Ni is then selectively evaporated above the n-type and p-type electrodes to prevent etching in subsequent processes. A thin photoresist film is then patterned with an array of circles packed in a polka-dot sequence, with a 2.5 μm diameter and a center-to-center spacing 3.5 μm minimum, respectively. This precedes the transfer of this pattern to the SiO<sub>2</sub> layer using a

standard  $\text{CHF}_3/\text{Ar}$  reactive-ion etch (RIE) process, acting as a secondary mask in further fabrication steps to overcome issues of etching-rate selectivity. The patterned 2D microhole array is then formed by etching through the active-region, using  $\text{Cl}_2/\text{Ar}$  inductively coupled plasma (ICP) etching via the 100 nm ITO current spreading layer (CSL). The undamaged n-type and p-type electrodes are then re-exposed using the same selective  $\text{SiO}_2$  RIE processing, previously concealed by the 20 nm Ni that is first removed simply using  $\text{NHO}_3$ .

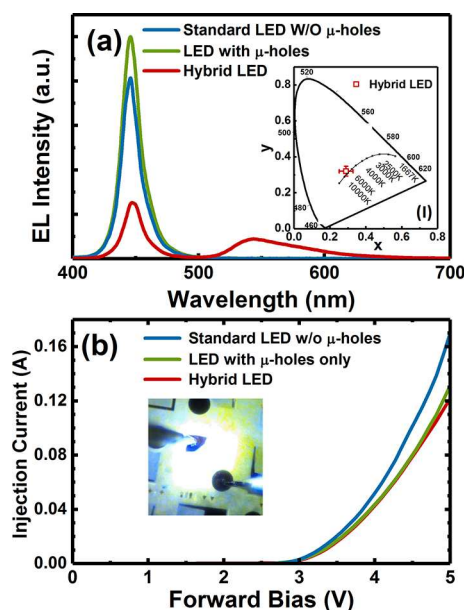
Figure 1b shows a scanning electron microscope (SEM) image taken at an angle of  $45^\circ$ , confirming a  $2.5 \mu\text{m}$  diameter hole with a 900 nm depth which is sufficient to completely expose the active-region side-walls and also demonstrating the continuity of the top p-contact. An etch-depth of just 390 nm is adequate to pass the InGaN/GaN MQWs of the as-grown LED wafer, where the measured 900 nm depth also includes the 250 nm  $\text{SiO}_2$  layer and the 100 nm ITO layer.

Figure 1c shows a high spatial-resolution PL mapping of the InGaN/GaN MQWs measured by a confocal PL system using a 375 nm diode laser as an excitation source, also exhibiting the same periodic pattern in PL intensity as the corresponding 2D microhole arrays. The complete absence of PL emission from the microhole regions also verifies the exposure of the active-region side-walls as is necessary to create a nonradiative FRET interaction volume. The trenches (between some microholes) as shown in the confocal PL mapping indicate a variation in intensity, which is mainly due to a fluctuation in indium composition and quantum well thickness.<sup>20–23</sup>

A prerequisite of nonradiative FRET is the significant spectral overlap between the donor emission and the acceptor absorption energy to attain exciton coupling.<sup>5</sup> The  $\pi$ -conjugated yellow-emitting polyfluorene copolymer F8BT, poly[(9,9-dioctylfluorenyl-2,7-diyl)-*alt-co*-(1,4-benzo-{2,1',3}-thiadiazole)], has pronounced absorption peaks at 320 and 455 nm with a high fluorescent quantum yield and relative ambient stability.<sup>24</sup> More importantly, the F8BT emits a broad yellow peak confirmed by our absorption spectral measurements,<sup>5</sup> displaying an overall yellow appearance, and is therefore ideally suited in the application of hybrid white-LEDs demonstrating nonradiative FRET color-conversion. The top-down fabrication process is thus completed with the deposition of F8BT to fill into the arrayed microholes. Organic materials are highly susceptible to degradation in the presence of atmospheric moisture and oxygen, resulting in permanent emission quenching.<sup>25</sup> To mitigate this organic material processing is completed within an anaerobic ( $\text{O}_2 < 0.5 \text{ ppm}$ ) glovebox environment with hydrogen gas ( $\text{H}_2 < 5\%$  in nitrogen ( $\text{N}_2$ )).

In order to make accurate comparison, an electrically injected LED with a standard unpatterned planar structure is initially fabricated and full characterization measurements are then conducted. Afterward, the device undergoes the top-down 2D microhole array fabrication process stated above and then full characterization measurements are performed. Finally, the device with the 2D microhole array structure is completed with deposition of F8BT, filling the arrayed microholes and then forming the final hybrid inorganic/organic device.

Figure 2a presents the electroluminescence (EL) spectra of the LED device before and after the top-down 2D microhole array fabrication process (i.e., both without the deposition of F8BT), measured under a 20 mA injection current, indicating a slight improvement in EL intensity after the 2D microhole array fabrication process, which may relate to an increased light-extraction efficiency (LEE) as a result of the existence of the



**Figure 2.** (a) EL spectra of the standard planar blue LED, the reference blue LED and the final hybrid white LED measured at 20 mA injection current, where Inset shows a CIE 1931 chromaticity diagram with the coordinates of the hybrid white LED measured at 2 mA injection current; (b)  $I$ - $V$  characteristics of the standard planar blue LED, the reference blue LED and the final hybrid white LED, respectively, where inset shows an optical image of the white emission from the hybrid white LED at 20 mA injection current.

microhole arrays.<sup>26</sup> Figure 2a also shows the typical EL spectrum of the hybrid white LED measured under a 20 mA injection current. Both the blue-emission at 450 nm and the yellow-emission centered at 550 nm have been demonstrated with a 65% difference between them in EL intensity. An optical image of its EL emission as shown in the inset of Figure 2b displays white light, measured at 20 mA.

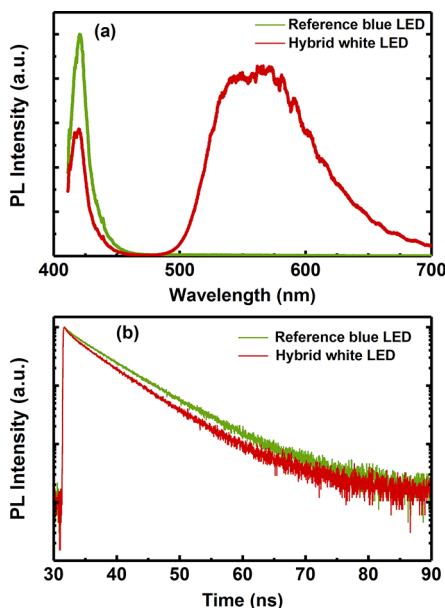
Chromaticity is then quantified using standardized Commission Internationale de l'Éclairage (CIE) calculations. A dichromatic color mixing allows generation of all CIE 1931 chromaticity coordinates between the two individual points through change in dominant emission,<sup>27</sup> where the blue InGaN/GaN LED and the F8BT polymer have respective (0.15, 0.04) and (0.42, 0.57) coordinates on the color-space diagram.<sup>28</sup> For an example, inset in Figure 2a shows the typical CIE color coordinates of  $(0.29 \pm 0.039, 0.32 \pm 0.027)$  and a color-correlated temperature of about 8336 K, measured at 2 mA injection current. This corresponds to a color rendering index (CRI) of  $\sim 53$ , which needs to be improved. This is achieved when the yellow-emitting F8BT polymer is drop-cast in a 5 mg/mL toluene concentrated solution, allowing this to naturally fill the microhole volume, improving the contribution of F8BT emission to the EL spectrum significantly. Of course, further optimization is still required in order to further increase CRI by tuning the concentration of F8BT in a toluene solution or decreasing the remaining blue-emission area by increasing the microhole density.

Figure 2b shows the  $I$ - $V$  characteristics, exhibiting that the electrical properties between the standard planar blue LED and the blue LED with the microhole array structure remain relatively unchanged. In detail, the LED with a microhole array structure exhibits only a small 90 mV increase in turn-on

voltage ( $V_0$ ) from 3.46 V compared with the standard planar LED.

Figure 2b also shows the  $I$ - $V$  characteristics of the hybrid LED and the reference blue LED (nonhybrid, i.e., the blue LED only with the 2D microhole array structure), demonstrating no discernible change in electrical properties after F8BT deposition, with an identical 3.55 V turn-on voltage and almost identical effects of series resistance with only a small 930 m $\Omega$  increase.<sup>29</sup>

Figure 3a shows the room-temperature PL spectra of the hybrid LED and the reference blue LED, both measured at



**Figure 3.** (a) PL spectra of the LED only with a microhole array structure and the hybrid white LED, respectively, both measured at room temperature; and (b) TRPL decay traces of the InGaN/GaN MQWs in the hybrid white LED and the reference blue LED, respectively.

room temperature using a 375 nm diode laser as an excitation source. The reference blue LED shows a strong PL emission peak in the blue spectral region, while the hybrid LED clearly demonstrates a broad second peak from the F8BT in the yellow region in addition to the blue emission from the InGaN/GaN MQWs. Figure 3a also provides an initial evidence of the nonradiative FRET with a 42% quenching of the InGaN/GaN MQW emission by comparing the PL spectra of the two LED devices, as we observed previously.<sup>5,30</sup>

Nonradiative FRET is typically investigated using time-resolved PL (TRPL) measurements by examining a change in the MQW exciton dynamics of the same structured LED device with and without nonradiative FRET.<sup>5,29–34</sup> TRPL measurements have been performed on both the hybrid LED and the reference blue LED. These measurements are carried out using a time-correlated single photon counting (TCSPC) system, where a 375 nm pulsed laser-diode with a 50 ps pulse-width is used as an excitation source. The PL emission is dispersed using a Horiba iHR550 monochromator and is then detected with a Hamamatsu hybrid photodetector at the emission peak from the InGaN/GaN MQWs. The system with a response-time of 150 ps is time-correlated using a Becker & Hickl SPC-130 acquisition module. TRPL measurements have been conducted on the two devices in an optical cryostat under

10<sup>-6</sup> Torr vacuum at room-temperature. This eliminates as far as is reasonably practicable the effects of photo-oxidation in the organic material, with a combined negligible exposure to air and background light irradiation. A low excitation power density is maintained throughout to minimize any possible many-body effects, ensuring excitonic recombination mechanics dominate the measured decay.<sup>5</sup>

Figure 3b presents the typical room temperature TRPL decay traces of the InGaN/GaN MQWs in the hybrid LED and the reference blue LED, showing a clear reduction in decay lifetime ( $k^{-1}$ ) for the hybrid LED compared with the reference blue LED. This reduction cannot be observed if there are not any nonradiative FRET processes involved.<sup>6</sup> A large number of measurements have been repeatedly performed, demonstrating a consistent decrease in decay lifetime. In detail, a nonradiative FRET rate between the F8BT and the InGaN/GaN MQWs can be obtained by extracting a change in decay lifetime measured from the hybrid LED and the reference blue LED.

The decay parameters can be extracted from a standard biexponential fit, as defined in eq 1, where a two-component PL decay is described as having two decay elements, attributed first to the relaxation of localized excitons and second the exciton relaxation of free-carriers and localized states,<sup>35</sup> where  $\alpha_x$  and  $\tau_x$  define the individual magnitude and decay lifetime of the two terms. Furthermore, the decay rate is equal to  $k_x = \tau_x^{-1}$

$$I(t) = \alpha_1 \exp\left(-\frac{t}{\tau_1}\right) + \alpha_2 \exp\left(-\frac{t}{\tau_2}\right) \quad (1)$$

The decay rate of a bare InGaN/GaN LED ( $k_{\text{MQW}}$ ) is dependent on radiative ( $k_r$ ) and nonradiative ( $k_{\text{nr}}$ ) recombination rates, as is given in eq 2.

$$k_{\text{MQW}} = k_r + k_{\text{nr}} \quad (2)$$

Nonradiative FRET coupling in a hybrid device generates a change in decay dynamics, in that an additional energy transfer channel is present, meaning that the total recombination rate ( $k_{\text{hyb}}$ ) requires modification in order to include a nonradiative FRET ( $k_{\text{FRET}}$ ) decay term, as in eq 3.<sup>5</sup>

$$k_{\text{hyb}} = k_r + k_{\text{nr}} + k_{\text{FRET}} \quad (3)$$

The efficiency of the nonradiative FRET process can ultimately be determined from the measured difference in decay rates between the hybrid LED and the reference blue LED, isolating the FRET rate. This is a standard approach widely used.<sup>5,6,9,12,28–34</sup>

The average weighted lifetime ( $\bar{\tau}$ ) of a biexponential decay, calculated using eq 4,<sup>36</sup> results in a typical decrease from 6.7 ns for the reference blue LED to 5.5 ns for the hybrid LED, obtained by fitting the TRPL decay traces as shown in Figure 3b. This then corresponds to an enhanced decay rate as a result of the nonradiative FRET process from  $k_{\text{MQW}} = 0.15 \text{ ns}^{-1}$  to  $k_{\text{hyb}} = 0.18 \text{ ns}^{-1}$ , isolating a  $0.03 \text{ ns}^{-1}$  FRET rate that produces a 16.7% FRET efficiency.

$$\bar{\tau} = \frac{\alpha_1 \tau_1^2 + \alpha_2 \tau_2^2}{\alpha_1 \tau_1 + \alpha_2 \tau_2} \quad (4)$$

It is also worth highlighting that the FRET efficiency is often corrected by averaging across the active FRET interaction area.<sup>5,33</sup> A corrected FRET efficiency is therefore significantly increased but is not calculated here.<sup>5,30</sup> The FRET interaction area of an individual microhole can be determined by

anticipating a 10 nm dipole–dipole separation following the microhole circumference, outside which the nonradiative FRET cannot occur. Using this assumption and other known dimensions, it can be reliably estimated that only 0.64% of the device volume can contribute to the highly efficient nonradiative FRET process. The relatively small area in which recombination is dominated by the fast-acting FRET process between the InGaN/GaN MQWs and the F8BT highlights the enhancement in down-converted yellow-emission. The corrected FRET efficiency will be significantly increased as expected.<sup>5,30</sup>

In summary, an electrically injected hybrid organic/inorganic III-nitride white LED has been demonstrated with an architecture compatible with the near-field requirements of nonradiative FRET, providing an increased dipole–dipole proximity. A top-down 2D microhole array structure is transferred to the InGaN/GaN MQW of a standard blue planar-LED using a novel combination of a standard fabrication process that results in a device with relatively unchanged electrical performance. A white-light EL emission has been achieved with typical CIE color coordinates at (0.29, 0.32). TRPL measurements reveal a consistent reduction in carrier recombination lifetime of the InGaN/GaN MQWs in our hybrid device, confirming the nonradiative FRET process occurring between the InGaN/GaN MQWs and the F8BT. The nonradiative FRET process contributes a 16.7% FRET efficiency across a device in which it can account for 0.64% of the total interaction area, suppressing likely nonradiative recombination processes and therefore enhancing total device efficiency.

## AUTHOR INFORMATION

### Corresponding Author

\*E-mail: t.wang@sheffield.ac.uk.

### Notes

The authors declare no competing financial interest.

## ACKNOWLEDGMENTS

Financial support is acknowledged from the Engineering and Physical Sciences Research Council (EPSRC), U.K., via EP/M003132/1 and EP/P006973/1

## REFERENCES

- (1) Chow, W.; Yeh, C. H.; Liu, Y. F.; Liu, Y. Improved modulation speed of LED visible light communication system integrated to main electricity network. *Electron. Lett.* **2011**, *47*, 867–868.
- (2) Vučić, J.; Kottke, C.; Nerreter, S.; Buttner, A.; Langer, K.-D.; Walewski, J. W. White Light Wireless Transmission at 200+Mb/s Net Data Rate by Use of Discrete-Multitone Modulation. *IEEE Photonics Technol. Lett.* **2009**, *21*, 1511–1513.
- (3) Laurand, N.; Guilhabert, B.; McKendry, J.; Kelly, A. E.; Rae, B.; Massoubre, D.; Gong, Z.; Gu, E.; Henderson, R.; Dawson, M. D. Colloidal quantum dot nanocomposites for visible wavelength conversion of modulated optical signals. *Opt. Mater. Express* **2012**, *2*, 250–260.
- (4) Agranovich, V. M.; Gartstein, Y. N.; Litinskaya, M. Hybrid Resonant Organic–Inorganic Nanostructures for Optoelectronic Applications. *Chem. Rev.* **2011**, *111*, 5179–5214.
- (5) Smith, R.; Liu, B.; Bai, J.; Wang, T. Hybrid III-Nitride/Organic Semiconductor Nanostructure with High Efficiency Nonradiative Energy Transfer for White Light Emitters. *Nano Lett.* **2013**, *13*, 3042–3047.
- (6) Achermann, M.; Petruska, M. A.; Kos, S.; Smith, D. L.; Koleske, D. D.; Klimov, G. C. Energy-transfer pumping of semiconductor

nanocrystals using an epitaxial quantum well. *Nature* **2004**, *429*, 642–646.

(7) Kos, S.; Achermann, M.; Klimov, V. I.; Smith, D. L. Different regimes of Förster-type energy transfer between an epitaxial quantum well and a proximal monolayer of semiconductor nanocrystals. *Phys. Rev. B: Condens. Matter Mater. Phys.* **2005**, *71*, 205309.

(8) Agranovich, V. M.; Basko, D. M.; La Rocca, G. C.; Bassani, F. Excitons and optical nonlinearities in hybrid organic-inorganic nanostructures. *J. Phys.: Condens. Matter* **1998**, *10*, 9369–9400.

(9) Achermann, M.; Petruska, M. A.; Koleske, D. D.; Crawford, M. H.; Klimov, V. I. Nanocrystal-Based Light-Emitting Diodes Utilizing High-Efficiency Nonradiative Energy Transfer for Color Conversion. *Nano Lett.* **2006**, *6*, 1396–1400.

(10) Blumstengel, S.; Sadofev, S.; Xu, C.; Puls, J.; Henneberger, F. Converting Wannier into Frenkel excitons in an inorganic/organic hybrid semiconductor nanostructure. *Phys. Rev. Lett.* **2006**, *97*, 237401.

(11) Heliotis, G.; Itskos, G.; Murray, R.; Dawson, M. D.; Watson, I. M.; Bradley, D. D. C. Hybrid Inorganic/Organic Semiconductor Heterostructures with Efficient Non-Radiative Energy Transfer. *Adv. Mater.* **2006**, *18*, 334–338.

(12) Rindermann, J. J.; Pozina, G.; Bonemar, M.; Hultman, L.; Amano, H.; Lagoudakis, P. Dependence of Resonance Energy Transfer on Exciton Dimensionality. *Phys. Rev. Lett.* **2011**, *107*, 236805.

(13) Itskos, G.; Belton, C. R.; Heliotis, G.; Watson, I. M.; Dawson, M. D.; Murray, R.; Bradley, D. D. C. White light emission via cascade Förster energy transfer in (Ga, In)N quantum well/polymer blend hybrid structures. *Nanotechnology* **2009**, *20*, 275207–275207.

(14) Andrews, D. L. A unified theory of radiative and radiationless molecular energy transfer. *Chem. Phys.* **1989**, *135*, 195–201.

(15) Andrews, D. L.; Bradshaw, D. S. Virtual photons, dipole fields and energy transfer: a quantum electrodynamical approach. *Eur. J. Phys.* **2004**, *25*, 845–858.

(16) Sahoo, H. Förster Resonance Energy Transfer - A Spectroscopic Nanoruler: Principle and Applications. *J. Photochem. Photobiol., C* **2011**, *12*, 20–30.

(17) Findlay, N. J.; Bruckbauer, J.; Inigo, A. R.; Breig, B.; Arumugam, S.; Wallis, D. J.; Martin, R. W.; Skabara, P. J. An organic down-converting material for white-light emission from hybrid LEDs. *Adv. Mater.* **2014**, *26*, 7290–7294.

(18) Guha, S.; Haight, R. a.; Bojarczuk, N. a.; Kisker, D. W. Hybrid Organic–inorganic Semiconductor-Based Light-Emitting Diodes. *J. Appl. Phys.* **1997**, *82*, 4126.

(19) Hide, F.; Kozodoy, P.; DenBaars, S. P.; Heeger, A. J. White Light from InGaN/conjugated Polymer Hybrid Light-Emitting Diodes. *Appl. Phys. Lett.* **1997**, *70*, 2664.

(20) Jeong, M. S.; Kim, J. Y.; Kim, Y.-W.; White, J. O.; Suh, E.-K.; Hong, C.-H.; Lee, H. J. Spatially Resolved Photoluminescence in InGaN/GaN Quantum Wells by near-Field Scanning Optical Microscopy. *Appl. Phys. Lett.* **2001**, *79*, 976–978.

(21) Okamoto, K.; Choi, J.; Kawakami, Y.; Terazima, M.; Mukai, T.; Fujita, S. Submicron-Scale Photoluminescence of InGaN/GaN Probed by Confocal Scanning Laser Microscopy. *Jpn. J. Appl. Phys.* **2004**, *43*, 839–840.

(22) Okamoto, K.; Kaneta, A.; Kawakami, Y.; Fujita, S.; Choi, J.; Terazima, M.; Mukai, T. Confocal Microphotoluminescence of InGaN-Based Light-Emitting Diodes. *J. Appl. Phys.* **2005**, *98*, 64503.

(23) Bruckbauer, J.; Edwards, P. R.; Sahonta, S.-L.; Massabuau, F. C.-P.; Kappers, M. J.; Humphreys, C. J.; Oliver, R. A.; Martin, R. W. Cathodoluminescence Hyperspectral Imaging of Trench-like Defects in InGaN/GaN Quantum Well Structures. *J. Phys. D: Appl. Phys.* **2014**, *47*, 135107.

(24) Lane, P. A. Polyfluorene Electroluminescence. In *Org. Light. Devices A Surv.* Shinar, J., Ed.; Springer-Verlag: New York, 2004; pp 265–299.

(25) Linde, S.; Shikler, R. Comprehensive study of the influence of different environments on degradation processes in F8BT: Correlating optoelectronic properties with Raman measurements. *J. Appl. Phys.* **2013**, *114*, 164506.

- (26) Sun, B.; Zhao, L.; Wei, T.; Yi, X.; Liu, Z.; Wang, G.; Li, J. Shape designing for light extraction enhancement bulk-GaN light-emitting diodes. *J. Appl. Phys.* **2013**, *113*, 243104.
- (27) Schubert, E. F. *Light-Emitting Diodes*; Cambridge University Press: Cambridge, 2003.
- (28) Belton, C. R.; Itskos, G.; Heliotis, G.; Stavrinou, P. N.; Lagoudakis, P. G.; Lupton, J.; et al. New light from hybrid inorganic–organic emitters. *J. Phys. D: Appl. Phys.* **2008**, *41*, 94006.
- (29) Zhuang, Z.; Guo, X.; Liu, B.; Hu, F.; Li, Y.; Tao, T.; et al. High Color Rendering Index Hybrid III-Nitride/Nanocrystals White Light-Emitting Diodes. *Adv. Funct. Mater.* **2016**, *26*, 36–43.
- (30) Smith, R. M.; Athanasiou, M.; Bai, J.; Liu, B.; Wang, T. Enhanced non-radiative energy transfer in hybrid III-nitride structures. *Appl. Phys. Lett.* **2015**, *107*, 121108.
- (31) Xu, X.; Wang, H. Resonant Energy Transfer between Patterned InGaN/GaN Quantum Wells and CdSe/ZnS Quantum Dots. *Nanoscale* **2016**, *8*, 342–347.
- (32) Krishnan, C.; Brossard, M.; Lee, K.-Y.; Huang, J.-K.; Lin, C.-H.; Kuo, H.-C.; Charlton, M. D. B.; Lagoudakis, P. G. Hybrid Photonic Crystal Light-Emitting Diode Renders 123% Color Conversion Effective Quantum Yield. *Optica* **2016**, *3*, 503.
- (33) Chanyawadee, S.; Lagoudakis, P. G.; Harley, R. T.; Charlton, M. D. B.; Talapin, D. V.; Huang, H. W.; Lin, C. H. Increased Color-Conversion Efficiency in Hybrid Light-Emitting Diodes Utilizing Non-Radiative Energy Transfer. *Adv. Mater.* **2010**, *22*, 602–606.
- (34) Nizamoglu, S.; Guzelturk, B.; Jeon, D.-W.; Lee, I.-H.; Demir, H. V. Efficient Nonradiative Energy Transfer from InGaN/GaN Nanopillars to CdSe/ZnS Core/shell Nanocrystals. *Appl. Phys. Lett.* **2011**, *98*, 163108.
- (35) Feng, S. W.; Cheng, Y. C.; Liao, C. C.; Chung, Y. Y.; Liu, C. W.; et al. Two-Component Photoluminescence Decay in InGaN/GaN Multiple Quantum Well Structures. *Phys. Phys. Status Solidi B* **2001**, *228*, 121–124.
- (36) Lakowicz, J. R. *Princ. Fluoresc. Spectrosc.*; Springer US, 2006; pp 141–142.